Bioprocess Engineering ■■ (1999) ■■■ - ■■■

Bifurcation and chaos for a mutating autocatalator in a CSTR

A.E. Abasaeed

Abstract In this paper, we develop a conceptual model for autocatalytic reactions in which the autocatalyst undergoes a mutation process in a completely stirred tank reactor. Three cases with different mutation coefficient, α, and mutation efficiency, β, have been considered. The analysis of these cases shows the importance of the two parameters and the complexity of the resulting bifurcation diagrams. Co-existence of a mushroom and an isola have been determined for the first case. The isola portion is a low main product yield solution and is to be avoided. A sub-region of 7 co-existing steady states, with three stable static branches, has been determined for the second case. Chaos developing through period doubling and type 1 intermittency has been shown to occur for a fourth case.

List of symbols

A	desired product concentration
A_f	desired product concentration in feed
B	mutant concentration
B_f	mutant concentration in feed
k_1, k_2	rate constants
S	substrate concentration
S_f	feed substrate concentration
X	substrate conversion
Y	dimensionless desired product concentration
Y_f	dimensionless desired product concentration in feed
Z	dimensionless mutant concentration
Z_f	dimensionless mutant concentration in feed
V	reactor volume
U_1, U_2	decomposition product concentrations

Greek letters

α	mutation coefficient
β	mutation efficiency
θ	residence time in reactor

Received: 19 April 1999

A.E. Abasaeed
Chemical Engineering Department,
King Saud University,
PO Box 800, Riyadh 11421, Saudi Arabia

1 Introduction

In recent years a great deal of research effort has been spent on studying the complex dynamic behavior (multiplicity, stability and chaos) of chemically reactive systems [1–5]. Most of the previous work, aiming at showing these exotic behaviors, was focused on non-linearities induced by the exponential dependence of the rate constant on temperature. Simple systems which exhibit and elucidate similar behaviors are of great importance as elegantly put by Alhumaizi and Aris [6] "there is a need for such systems in each discipline, not only as expression of the plenitude of nature, but also as places where the workers in that discipline can 'prove' their theorems, algorithms or applications". The simplest reactor in the chemical engineering field is the Completely Stirred Tank Reactor (CSTR) in which the reactants are continuously fed and product withdrawn from it. Vigorous mixing in the reactor provides the uniformity of its content.

Autocatalytic reactions taking place in an isothermal CSTR provide one of the simplest systems for bifurcation studies. The autocatalyst provides the system with the feedback necessary for multiplicity of steady states, sustained oscillations and possibly chaos. The two-reaction model (cubic autocatalysis, $A + 2B \rightarrow 3B$ and catalyst decay, $B \rightarrow C$) which was advanced and studied by Gray and Scott [7] provided a base for a number of studies that followed [6, 8–11]. Lynch showed that in the system ($A + 2B \rightarrow 3B$, $B \rightarrow C$ and $D + 2B \rightarrow 3B$) chaotic behavior occurs. Leach et al. [12] obtained complex behavior with the two-cell system ($A + 2B \rightarrow 3B$, $B \rightarrow C$ and $P \rightarrow A$). In general, very interesting results were obtained using the above mentioned Gray and Scott model and the various versions of the modified model.

In this preliminary investigation, we develop a model for an autocatalytic reaction. However, the autocatalyst was assumed to undergo a mutation process giving another form which can also undergo an autocatalytic reaction, thus competing with the original autocatalyst. The model was originally developed as an over-simplification of the formation of cancerous cells from healthy, reproducing cells. This should by no means be taken as a "close" description of the formation and reproduction of cancerous cells and their competition with healthy cells. It is merely an attempt to explore the tip of the iceberg of the mutation process. The model has a number of parameters in it, comprehensive analysis of the effect of all parameters is impossible. Therefore, the effect of the two most important parameters α (defined as a mutation coefficient)

and β (defined as a mutation efficiency) for a mutant free feed is presented here. The major emphasis of the paper is on the bifurcation behavior, however, a case in which chaos prevails is also presented. It is worthy of mentioning here that, this conceptual model can be reduced to the Gray and Scott [7] for certain parameters values.

2 The model

The conceptual autocatalytic reaction with mutation which is assumed to take place in an isothermal CSTR is depicted as follows.

Reaction scheme:

$S + 2A \xrightarrow{k_1} 3A$: (A replication),

$A \xrightarrow{k_2} U_1$: (A decay),

$S + 2A \xrightarrow{\alpha k_1} 2B + A$: (A mutation to B),

$S + 2B \xrightarrow{\beta k_1} 3B$: (B replication),

$B \xrightarrow{k_2/\beta} U_2$: (B decay).

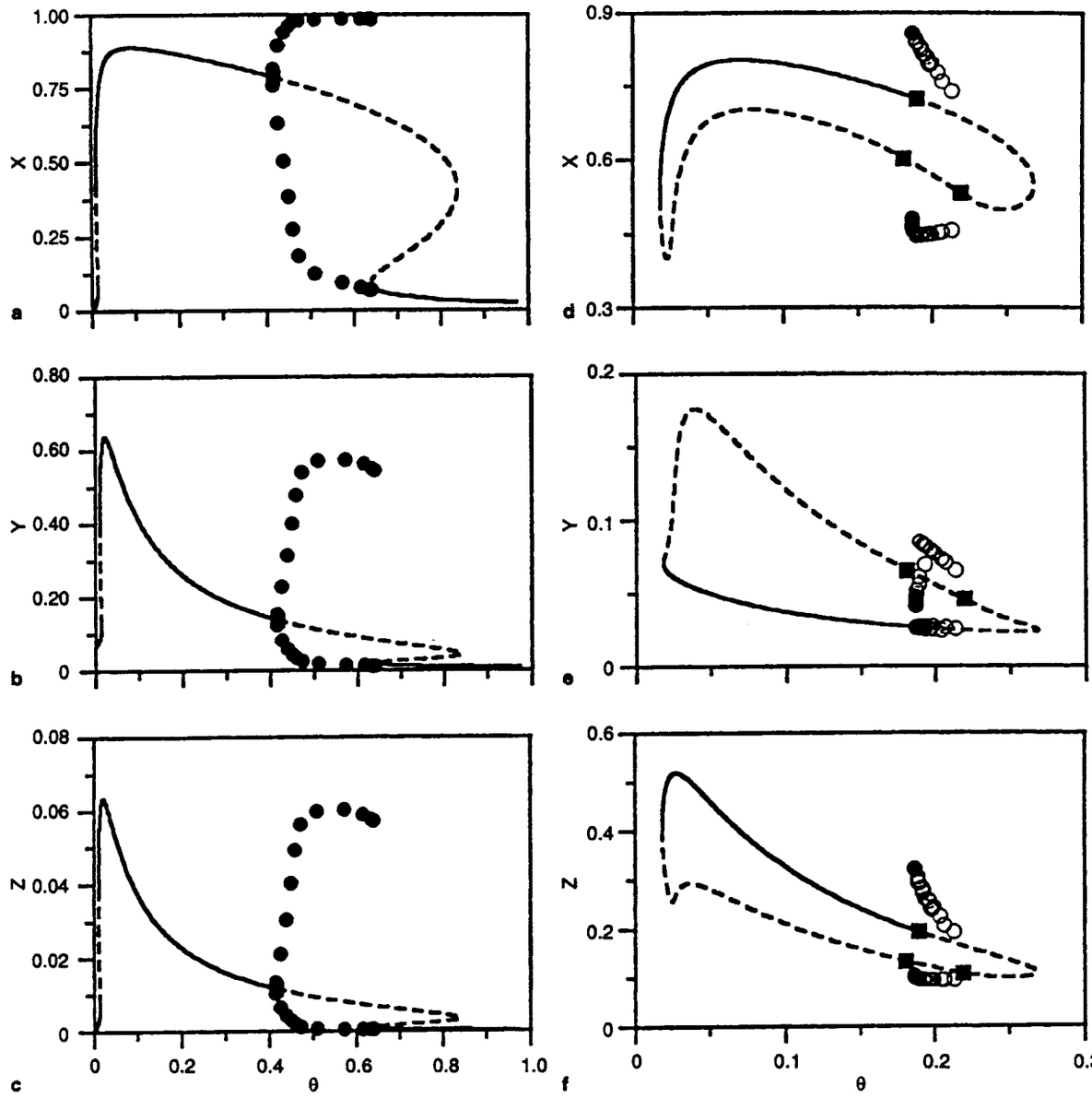

Fig. 1. Bifurcation diagram for case 1, $\alpha = 0.05$ and $\beta = 0.8$, for the mushroom (a) X vs. θ, (b) Y vs. θ and (c) Z vs. θ and for the isola (d) X vs. θ, (e) Y vs. θ and (f) Z vs. θ. [— = stable static, - - - - = unstable static, ■ = Hopf bifurcation point, ● = stable periodic, ○ = unstable periodic]

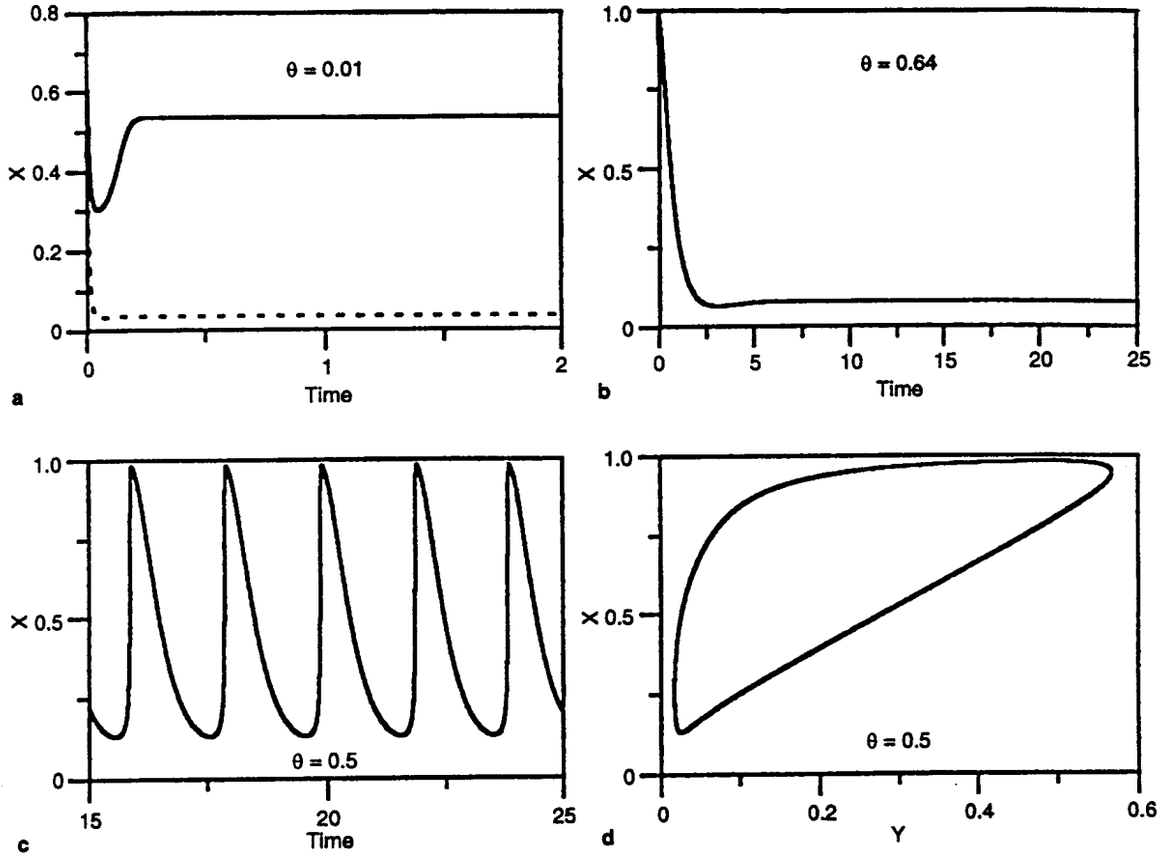

Fig. 2. Case 1: dynamic simulations for the mushroom (a) $\theta = 0.01$, (b) $\theta = 0.064$, (c) time trace at $\theta = 0.5$ and (d) phase plane at $\theta = 0.5$

Mass balance equations:
The mass balance equations are derived for the substrate (S), desired product (A) and the mutant (B).

The substrate (S):

$$V\frac{dS}{dt} = q(S_f - S) - Vk_1S\,A^2 - V\alpha.k_1S\,A^2 - V\beta.k_1S\,B^2 \quad . \tag{1}$$

The desired product (A):

$$V\frac{dA}{dt} = q(A_f - A) + Vk_1S\,A^2 - V\alpha.k_1S\,A^2 - Vk_2A \quad . \tag{2}$$

The mutant (B):

$$V\frac{dB}{dt} = q(B_f - B) + V\beta.k_1S\,B^2 + 2V\alpha.k_1S\,A^2 - V\frac{k_2}{\beta}B \quad . \tag{3}$$

Equations (1–3) can be transformed to Eqs. (4–6) respectively by defining the following quantities:

$$X = \frac{(S_f - S)}{S_f};\quad Y = \frac{A}{S_f};\quad Z = \frac{B}{S_f};$$

$$\gamma_1 = k_1.S_f^2;\ \text{and}\ \gamma_2 = k_2 \quad .$$

$$\frac{dX}{dt} = -\frac{X}{\theta} + (1+\alpha)\gamma_1(1-X)Y^2 + \beta.\gamma_1(1-X)Z^2 \quad , \tag{4}$$

$$\frac{dY}{dt} = \frac{(Y_f - Y)}{\theta} + (1-\alpha)\gamma_1(1-X)Y^2 - \gamma_2 Y \quad , \tag{5}$$

$$\frac{dZ}{dt} = \frac{(Z_f - Z)}{\theta} + \beta.\gamma_1(1-X)Z^2 + 2\alpha.\gamma_1(1-X)Y^2 - \frac{\gamma_2}{\beta}Z \quad . \tag{6}$$

3 Results and discussion

It is clear that the model equations include 7 parameters, namely: γ_1, γ_2, Y_f, Z_f, α, β and θ. For mutant-free feed, $Z_f = 0$. The values of the first three parameters, i.e., γ_1, γ_2 and Y_f are kept at 450, 11.25 and 0.067 respectively. The parameters α and β are varied to provide the cases under investigation. The parameter θ (space time) is used as the main bifurcation parameter. The bifurcation diagrams are constructed using the efficient continuation software developed by Doedel and Kernevez [13]. The Laypunov exponents are computed using the algorithm developed by Wolf et al. [14]. To ensure accuracy of the simulation results, the bound on the allowable error was maintained at 10^{-12}, with automatic step size integration routines. In regions where multiplicity of steady states occur, the set of initial conditions dictates the attractor to which the system

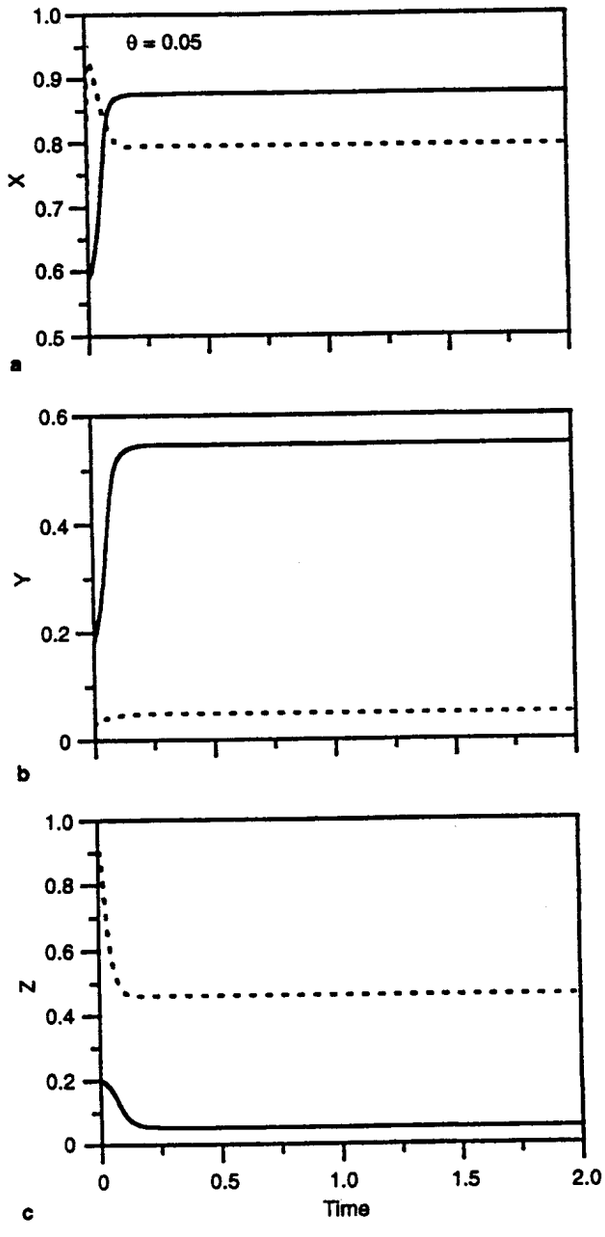

Fig. 3. Case 1: dynamic simulations for co-existing mushroom (solid lines) and isola (dashed lines), (a) X vs. time, (b) Y vs. time and (c) Z vs. time

tends to go. In this paper, four cases are presented: the first three cases concentrate on bifurcation behavior while the fourth case presents a brief account of chaotic behavior.

3.1
Case 1: (α = 0.05 and β = 0.8)

Figure 1 shows the bifurcation diagram with θ being the bifurcation parameter for $\alpha = 0.05$ and $\beta = 0.8$. The figure reveals that, there is a sub-region ($0.0181 \leq \theta \leq 0.268$) in which a bistability between a mushroom (Fig. 1a–c) and an isola (Figs. 1d–f) occurs.

For the mushroom attactor (Figs. 1a–c), as the value of the bifurcation parameter (θ) is increased from $\theta = 0$ to $\theta = 0.00944$ (corresponding to a limit or turning point) a unique stable static attractor exists. Between $\theta = 0.00944$ and $\theta = 0.0124$ (corresponding to a limit point), three steady states static branches (two stable branches and a middle unstable branch) exist. As illustrated in Fig. 2a, the dynamic simulation in this region (e.g. for $\theta = 0.01$) shows that the upper stable branch gives higher substrate conversion ($X = 0.536$) compared to the lower branch ($X = 0.0367$). The corresponding yield of the main product (Y) is also higher for the upper branch ($Y = 0.493$) compared to the lower branch ($Y = 0.09$). The corresponding mutant yield is low for both branches. Between $\theta = 0.0124$ and $\theta = 0.414$ (corresponding to a Hopf bifurcation point) a unique stable static attractor is present. In the range $0.414 \leq \theta \leq 0.638$ (corresponding to a limit point) there exists an unstable static attractor surrounded by a periodic attractor emanating from the Hopf bifurcation point as the only stable attactor. Dynamic simulation at $\theta = 0.5$ show the sustained oscillations of this periodic attractor as shown in Fig. 2c for time trace and Fig. 2d for phase plane. Between $\theta = 0.638$ and $\theta = 0.838$, three steady state solution branches exists (2 unstable and 1 stable). The simulation results shown in Fig. 2b reveals that this attactor is characterized by low conversion ($X = 0.08$) and low main product yield. For $\theta > 0.838$, the multiplicity of steady states vanishes and a unique stable static attractor exists in this region (Fig. 1a–c).

As clearly shown in Figs. 1a–c, the maximum substrate conversion ($X = 0.888$ as shown in Fig. 1a) occurs at $\theta = 0.09$ and the corresponding yield of the products is $Y = 0.43$ (Fig. 1b) and $Z = 0.04$ (Fig. 1c). The maximum main product yield ($Y = 0.64$ as shown in Fig. 1b) occurs at $\theta = 0.02$ for $X = 0.794$ and $Z = 0.063$. The mutant yield (Z) is low (<0.065) for all values of space time (θ) as seen in Fig. 1c.

For the isola attactor (Fig. 1d–f), the highest substrate conversion ($X = 0.8$) is achieved at $\theta = 0.071$ in a stable fashion. The corresponding product yield is $Y = 0.043$ and that of the mutant is $Z = 0.36$. The maximum product yield ($Y = 0.176$) is unstable and it occurs at $\theta = 0.039$ with higher mutant yield ($Z = 0.29$). The highest yield of the mutant ($Z = 0.52$) occurs at $\theta = 0.027$ at a substrate concentration of 0.73.

As mentioned previously, in the range $0.0181 \leq \theta \leq 0.268$ there is a bistability between the mushroom and the isola. Fig. 3 shows the bistability for $\theta = 0.05$. It is clear from the figure that higher substrate conversions resulting in higher main product yield are achieved when operating on the mushroom. The substrate conversion, product yield and mutant yield for the mushroom are respectively 0.877, 0.547 and 0.052 while those for the isola are 0.795, 0.05 and 0.46 respectively.

Fig. 4. Bifurcation diagram for case 2, $\alpha = 0.05$ and $\beta = 2$, (a) X vs. θ, (b) enlargement for $0 \leq \theta \leq 0.04$ and (c) enlargement showing 7 steady state branches and (d) enlargement for $0.61 \leq \theta \leq 0.64$. [— = stable static, - - - - = unstable static, ■ = Hopf bifurcation point, ● = stable periodic]

Fig. 5. Case 2: dynamic simulations X vs. time (a) tristability, $\theta = 0.0123$, (b) tristability, $\theta = 0.01$, (c) bistability, $\theta = 0.014$ and (d) bistability, $\theta = 0.635$

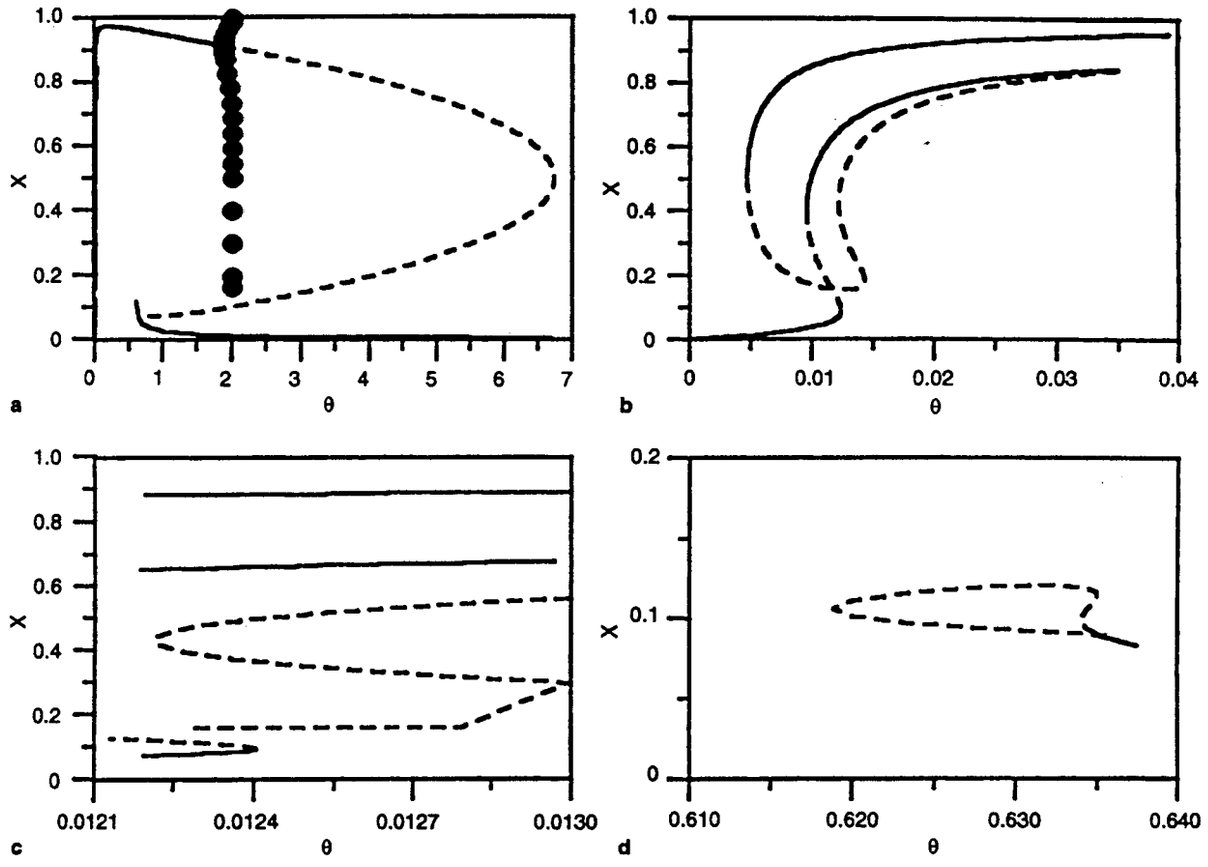
1.0
0.8
0.6
0.4
0.2
0
X
0 1 2 3 4 5 6 7
θ
a
0 0.01 0.02 0.03 0.04
θ
b
0.0121 0.0124 0.0127 0.0130
θ
c
0.2
0.1
0
0.610 0.620 0.630 0.640
θ
d

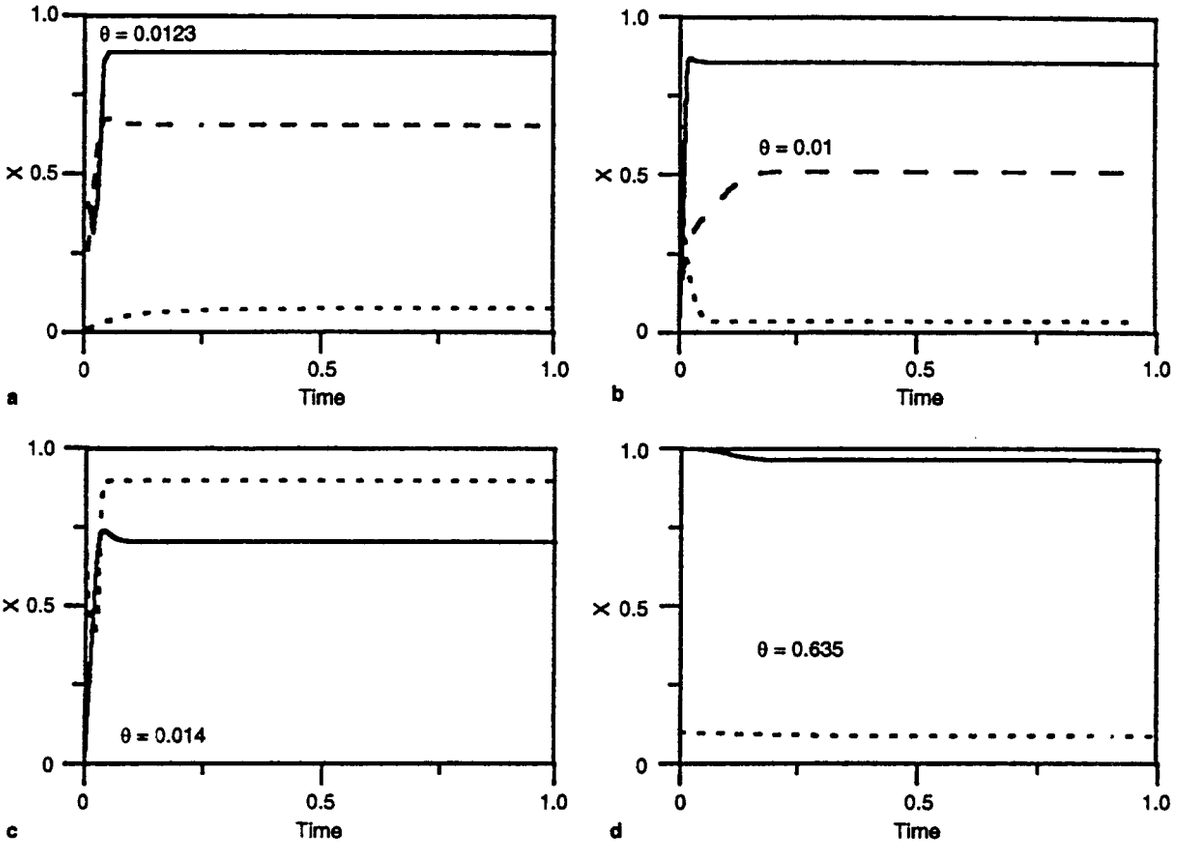
θ = 0.0123
θ = 0.01
θ = 0.014
θ = 0.635
X 0.5
0
0.5
1.0
Time
a
b
c
d

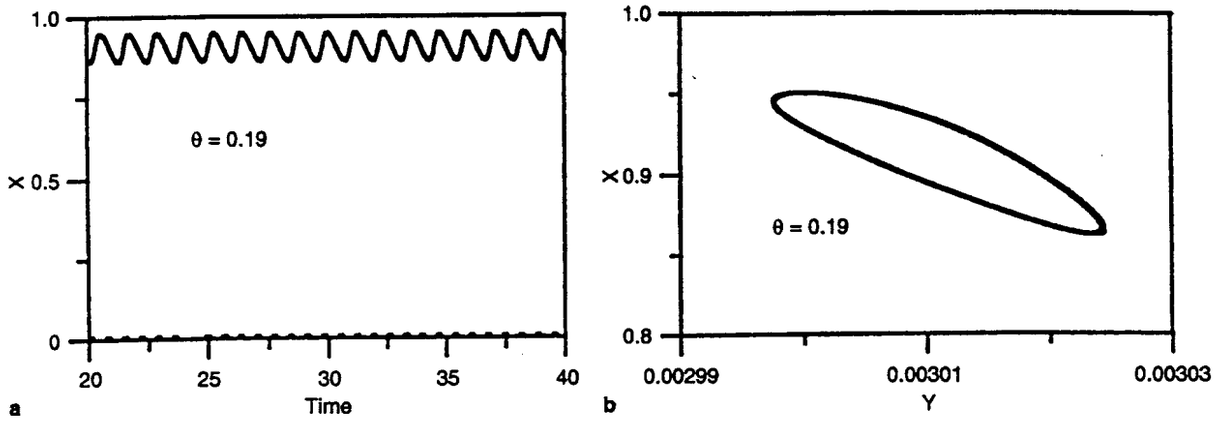

Fig. 6. Case 2: dynamic simulations (a) X vs. time, bistability (static and periodic), $\theta = 0.19$ and (b) X vs. Y, phase plane (periodic) $\theta = 0.19$

It is quite evident from the aforementioned discussion that if the system is operated to obtain higher main product yield, Y, with low mutant yield, Z, operation on the mushroom is more desirable and operation on the isola is to be avoided. Therefore, the effect of the two parameters (α and β) on the operation on the mushroom is analyzed for the following two cases (no isola is possible for the chosen values of α and β):

3.2
Case 2: ($\alpha = 0.05$ and $\beta = 2$)

Figure 4 shows the bifurcation diagram for X against θ (the Y and Z bifurcation diagrams are omitted for brevity). Fig. 4 is obtained for $\alpha = 0.05$ and $\beta = 2$ (which indicates higher mutation efficiency compared to case 1). The main features of the bifurcation diagram are:

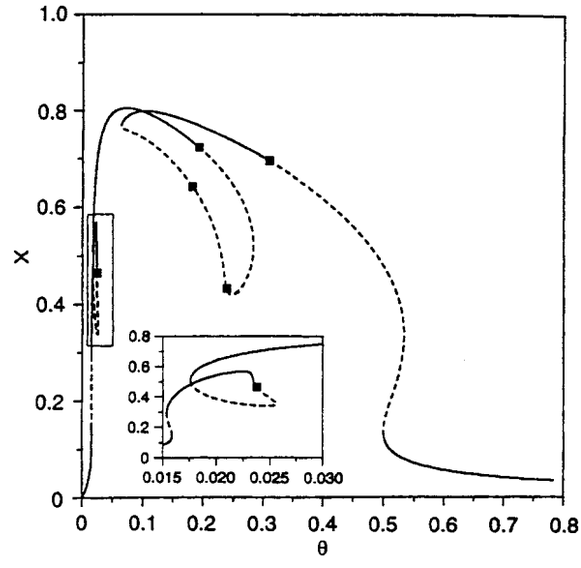

Fig. 7. Bifurcation diagram for X against θ for case 3, $\alpha = 0.175$ and $\beta = 0.8$. [—— = stable static, - - - - = unstable static, ■ = Hopf bifurcation point]

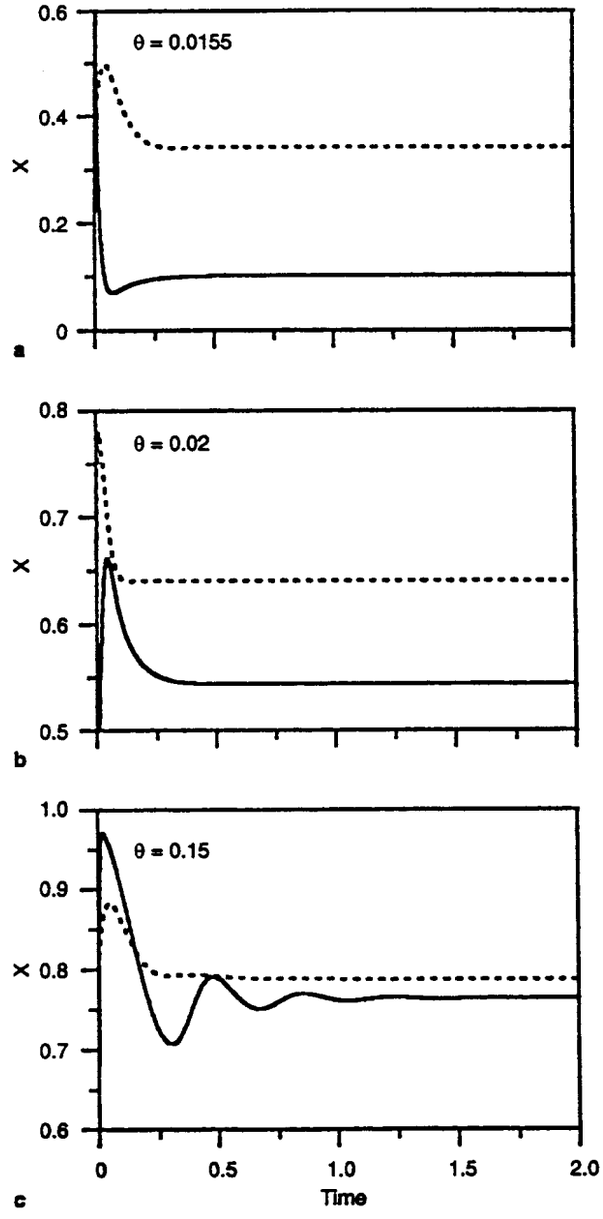

Fig. 8. Case 3: dynamic simulations showing bistability, X vs. time (a) $\theta = 0.0155$, (b) $\theta = 0.02$ and (c) $\theta = 0.15$

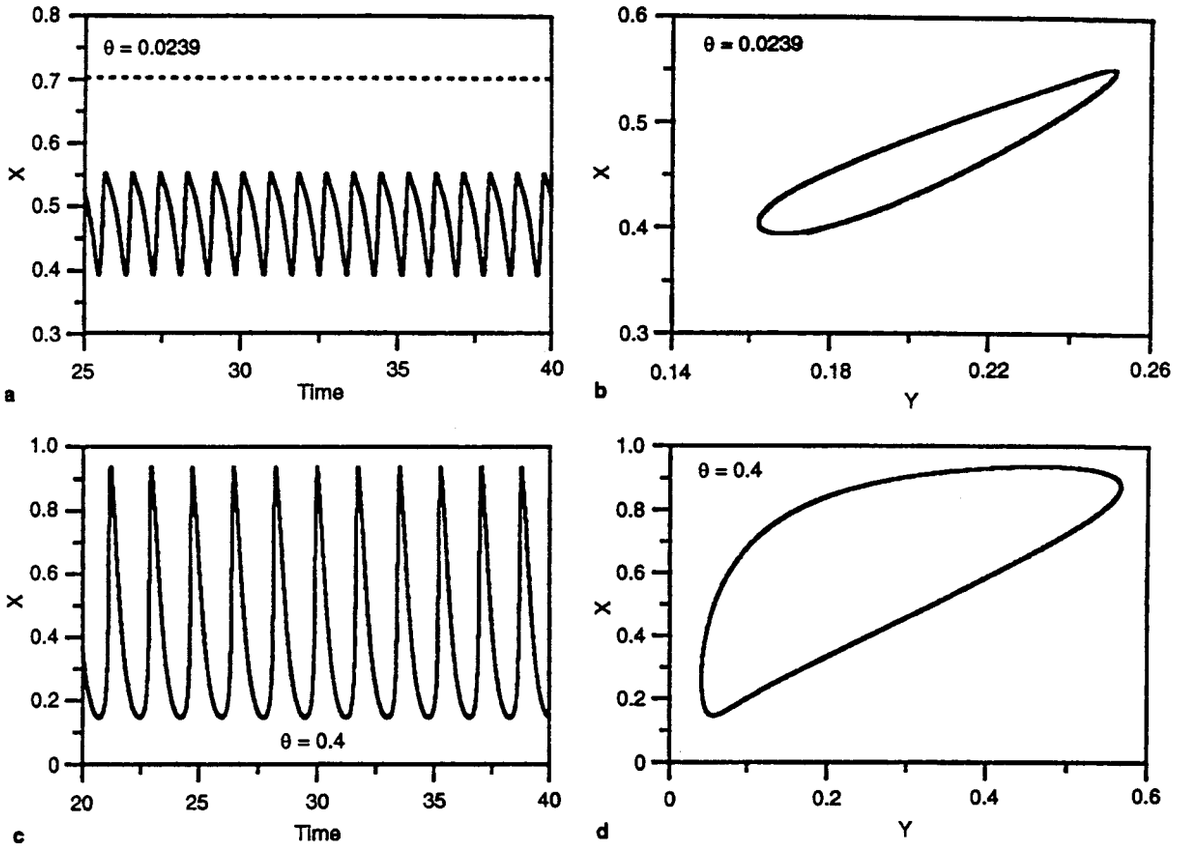

Fig. 9. Case 3: dynamic simulations (a) bistability, X vs. time $\theta = 0.0239$, (b) phase plane (periodic) at $\theta = 0.0239$, (c) X vs. time, $\theta = 0.4$ and (d) phase plane, $\theta = 0.4$

- The existence of 10 limit points.
- The presence of seven steady state static branches in the sub-region [$0.0122 < \theta < 0.0124$] as shown on the enlarged Fig. 4c. Three of these branches are stable and 4 unstable. Fig. 5a shows the results of the dynamic simulation at $\theta = 0.0123$ for the three stable steady state solutions. The steady state that gives the highest substrate conversion ($X = 0.883$) gives very low main product yield ($Y = 0.061$) and high mutant yield ($Z = 0.824$). The second steady state is characterized by reasonable substrate conversion ($X = 0.654$) with higher main product yield ($Y = 0.56$) compared to the mutant yield ($Z = 0.08$). The third steady state shows low conversion ($X = 0.076$), low product yield ($Y = 0.12$) and low mutant yield ($Z = 0.007$). Therefore, it is important to operate the system at the middle steady state branch in order to achieve higher main product (Y) and low mutant (Z) yields.
- Three sub-regions of five steady state static branches: 1 sub-region [$0.0096 < \theta < 0.0122$] with 3 stable branches and 2 sub-regions [$0.0124 < \theta < 0.0143$ and $0.634 < \theta < 0.6352$] with 2 stable branches each. The simulation results in the three sub-regions with multiple stable branches are shown in Fig. 5b–d. Figure 5b shows the tristability of steady states at $\theta = 0.01$ in the sub-region [$0.0096 < \theta < 0.0122$]. The X, Y and Z yields are (0.855, 0.062, and 0.81) for the highest substrate conversion branch, (0.51, 0.46 and 0.059) for the middle branch and (0.037, 0.09 and 0.0034) for the lower substrate conversion branch. Similar to the previous conclusion, it is advisable to operate at the middle branch for higher main product (Y) yield. The simulation results for the sub-region [$0.0124 < \theta < 0.0143$] are obtained at $\theta = 0.014$ as shown in Fig. 5c. This sub-region is characterized by the presence of two stable steady state branches. The higher substrate conversion steady state gives X, Y and Z of 0.9, 0.059 and 0.83 respectively whereas the lower conversion branch gives $X = 0.7$, $Y = 0.59$ and $Z = 0.08$. The main product yield ($Y = 0.59$) of the lower branch is even higher than the middle branch yield in $0.0096 < \theta < 0.0122$ ($Y = 0.46$). The second sub-region [$0.634 < \theta < 0.6352$] with two stable static branches is analyzed for $\theta = 0.635$. The high conversion branch ($X = 0.96$) gives low product yield ($Y = 0.008$) and the mutant yield is $Z = 0.21$ as shown in Fig. 5d. The other branch gives $X = 0.09$, $Y = 0.018$ and $Z = 0.0025$.
- Five sub-regions of three steady state static branches 3 sub-regions [$0.0047 < \theta < 0.0096$, $0.0143 < \theta < 0.034$ and $0.6352 < \theta < 1.89$] with 2 stable branches each and 2 sub-regions [$0.6168 < \theta < 0.634$ and $2 \ll \theta < 6.74$) with 1 stable branch each.
- One sub-region [1.89 (corresponding to a Hopf bifurcation point) $< \theta < 2.0$ (corresponding to homoclinic termination of the periodic branch)] of bistability between a steady states static branch and a periodic branch ema-

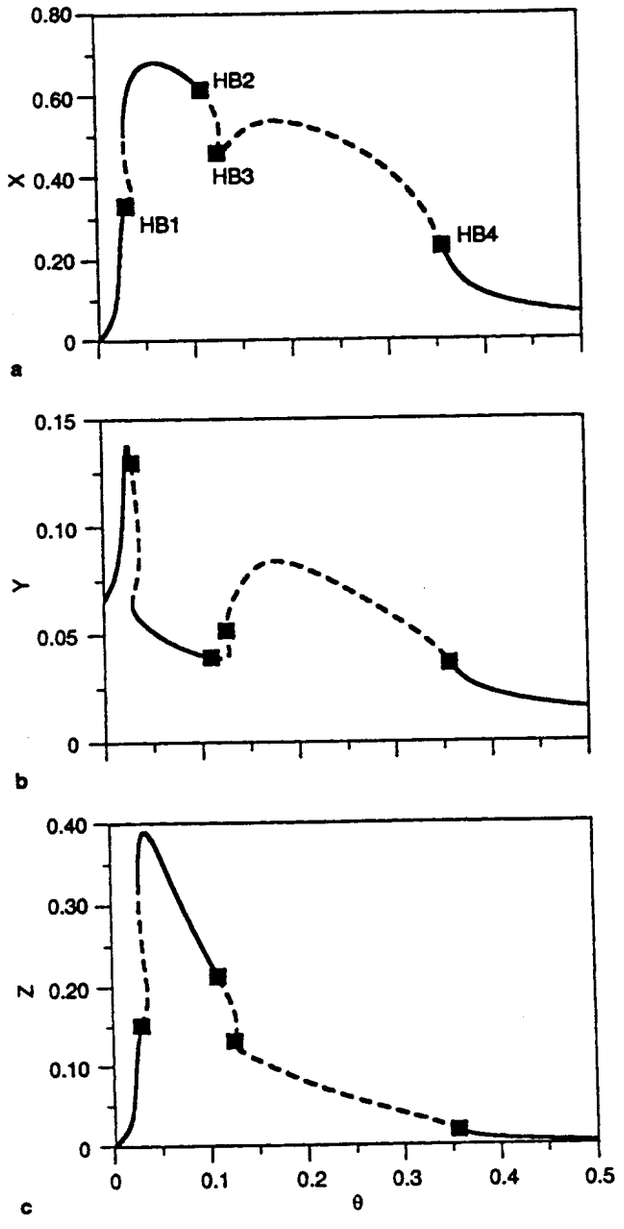

Fig. 10. Bifurcation diagram for X, Y and Z against θ for case 3, $\alpha = 0.29$ and $\beta = 0.68$ [— = stable static, - - - - = unstable static, ■ = Hopf bifurcation point]

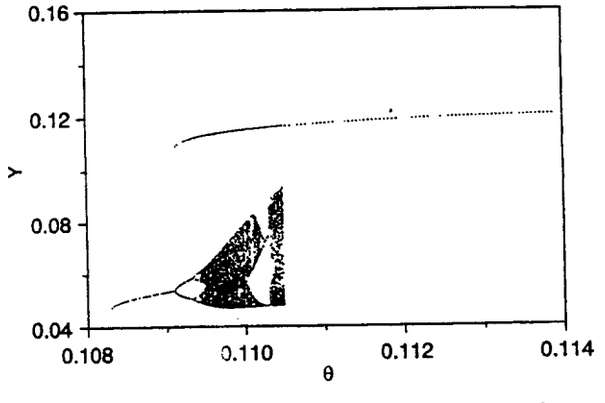

Fig. 11. Poincare bifurcation diagram for Y against θ

nating from the Hopf bifurcation point at $\theta = 1.89$. Time trace results obtained by dynamic simulation for the two attractors are shown in Fig. 6a whereas Fig. 6b shows the phase plane between X and Y for the periodic attractor. Both of these branches give low main product yield.

3.3
Case 3: ($\alpha = 0.175$ and $\beta = 0.8$)

The third case considered in this preliminary investigation is for $\alpha = 0.175$ (which indicates higher mutation coefficient compared to case 1) and $\beta = 0.8$. The bifurcation diagram relating the substrate conversion to space time, θ, is shown in Fig. 7. The small figure inside Fig. 7 is an enlargement for the sub-region $0.015 < \theta < 0.03$. The main features of the bifurcation diagram are:

- The existence of 8 turning (limit) points and 5 Hopf bifurcation points. Two stable periodic branches emanate from the Hopf bifurcation points at $\theta = 0.02373$ and $\theta = 0.03084$. The periodic branches emanating from the other three Hopf bifurcation points are unstable. For clarity purposes, all periodic branches are not shown in Fig. 7.
- Presence of six sub-regions of three steady state static branches. Three of these sub-regions ($0.01537 < \theta < 0.01586$, $0.01758 < \theta < 0.02373$ and $0.062627 < \theta < 0.19178$) have 2 stable branches and 1 unstable branch each. Each of the other three sub-regions ($0.02373 < \theta < 0.02557$, $0.19178 < \theta < 0.28269$ and $0.5 < \theta < 0.533$) have 1 stable branch and 2 unstable branches. The dynamic simulation results for the three sub-regions with 2 stable static branches each are shown in Fig. 8. Fig. 8a presents the simulation results at $\theta = 0.0155$ for the sub-region $0.01537 < \theta < 0.01586$. The higher substrate conversion steady state ($X = 0.342$) gives a main product yield of $Y = 0.235$ and mutant yield of $Z = 0.11$. The other branch has X, Y and Z of 0.101, 0.115 and 0.027 respectively. The results for the sub-region $0.01758 < \theta < 0.02373$ is shown in Fig. 8b for $\theta = 0.02$. The two attractors have X, Y and Z of (0.641, 0.063 and 0.492 represented by the dashed line) and (0.544, 0.295 and 0.195 represented by the solid line) respectively. The result for the last sub-region ($0.062627 < \theta < 0.19178$) with 2 stable attractors is shown in Fig. 8c. The conversion, X, and the two yields, Y and Z at $\theta = 0.15$ for the 2 attractors are (0.788, 0.2 and 0.103) and (0.764, 0.03 and 0.242) respectively. It is worth mentioning here that, while the conversion for the last case ($\theta = 0.15$) is about the same, the main product yield is quite different.
- One sub-region ($0.02373 < \theta < 0.0251$) of a bistabilty between a static and a periodic attractor. The simulation results at $\theta = 0.0239$ are shown in Fig. 9a for the two attractors. The static attractor gives low main product yield, $Y = 0.06$, and high mutant yield $Z = 0.52$ at a conversion of $X = 0.7$. Figure 9b is a phase plane for the periodic attractor. It shows that as the conversion oscillates between $0.4 < X < 0.55$, the main product yield oscillates between $0.16 < Y < 0.256$.
- The other sub-regions in the bifurcation diagram have a unique stable attractor (mainly static attractors and one periodic). The periodic attractor covers the sub-region

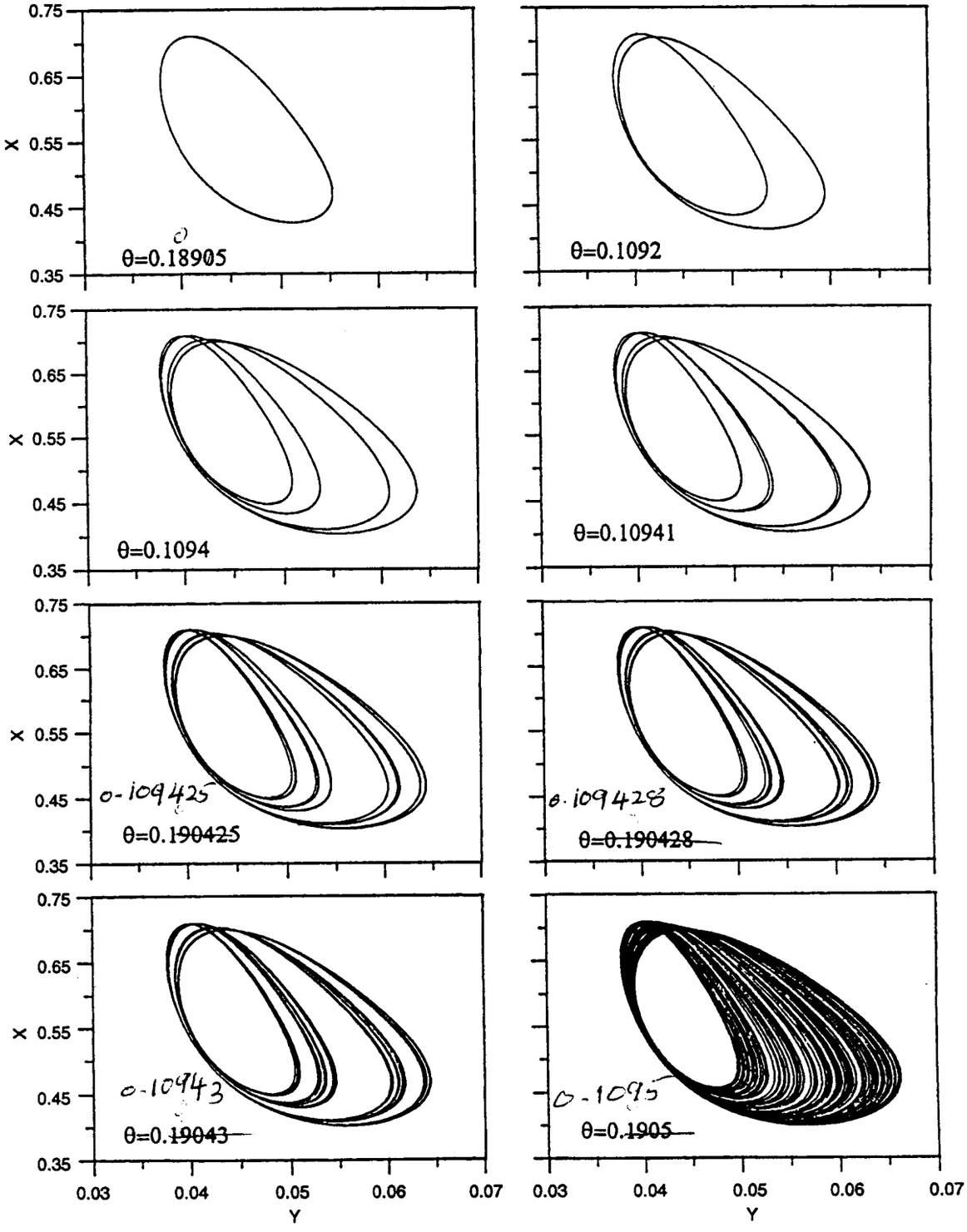

Fig. 12. Development of chaos through period doubling. Phase planes for X against Y for various θ values

$\theta = 0.3084$ (corresponding to a Hopf bifurcation point) and $\theta = 0.5$ (corresponding to homoclinic termination of the periodic branch). Figure 9c (for time trace) and Fig. 9d (for phase plane) illustrate the simulation results at $\theta = 0.4$. The sustained oscillations are evident from the figures and the main product yield oscillates in $0.04 < Y < 0.28$.

3.4 Case 4: ($\alpha = 0.29$ and $\beta = 0.68$)

The past three cases elucidated the importance of the parameters α and β on the bifurcation behavior. In the fourth case, the values of α and β are chosen such that chaos prevails in the system. Fig. 10 shows the bifurcation diagram for the conversion, X, the main product

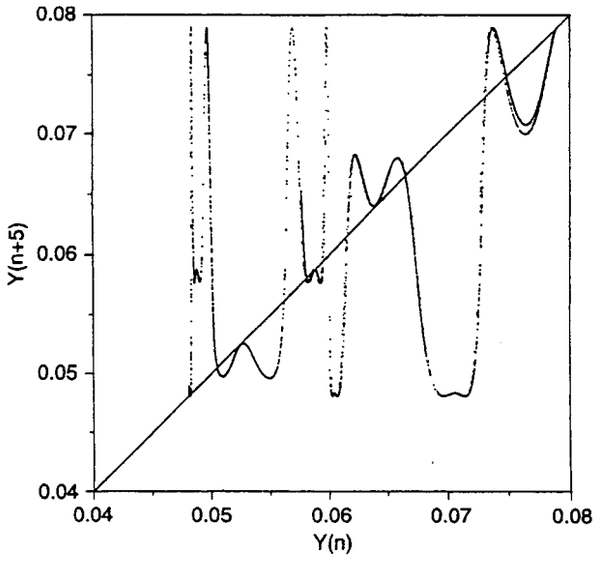

Fig. 13. Development of chaos through type 1 intermittency. Fifth iterate map at $\theta = 0.109929$

yield, Y, and the mutant yield, Z. As in previous cases, θ is the bifurcation parameter. The figure shows the existence of 4 Hopf bifurcation points and 4 limit points. The stable yield of the main product is higher than that of the mutant for relatively low (before HB1) and high (after HB4) values of θ. The periodic branches emanating (not shown on the figure) from the Hopf bifurcation points are (a) from HB1 terminates homoclinically on the saddle branch (b) from HB2 undergoes period doubling bifurcations giving chaos with a number of sandwitched periodic windows (Fig. 11) and will be discussed in some details later (c) from HB3 terminates homoclinically on the saddle branch and (d) from HB4 continues a period 1 attractor until it loses stability close to HB2, thus coexisting with the attractor from HB2 for some values of θ as shown in Fig. 11.

Figure 11 shows a one parameter Poincare bifurcation diagram for Y against θ. The plot gives the intersections of Y (in one direction) with the plane $X = 0.5$ and $Z > 0$. Development of chaos through period doubling and regaining of periodicity through period halving is clear from the figure. A clearer picture for the period doubling mechanism (P1 → P2 → P4 → P8 → P16 →... chaos) is presented in Fig. 12 for phase planes as chaos develops with θ. The largest Lyapunov exponent was positive for $\theta = 0.1905$ which confirms chaotic behavior of this attractor.

Sandwitched inside the chaotic attractor of Fig. 11 are a number of periodic windows. Intermittency is a term used to describe the presence of laminar channels (periodic oscillations) which are sandwiched inside chaotic bursts [15]. Type 1 intermittency (occurs when the Floquet multiplier exits the unit circle through +1) can be determined by plotting the ith iterate map [15, 16]. The 5th iterate map for the product yield, Y, is plotted in Fig. 13. It is clear from this figure that the curve approaches the bisectrix tangentially at 5 distinct points which confirms the type 1 intermittency for this case.

4 Conclusions

A simplified model for autocatalytic reactions taking place in a CSTR has been developed. The autocatalyst undergoes mutation. The mutant competes with the autocatalyst for the limiting substrate necessary for their replication. Both species undergo a decay process. The bifurcation diagrams are constructed for 4 representative values of the two most important parameters α and β. The first three cases concentrate on bifurcation behavior while the forth shows chaotic behavior developing through period-doubling and type 1 intermittency.

References

1. **Balakotaiah, V.; Luss, D.:** Multiplicity Criteria for Multiple-Reaction Network. A.I.Ch.E.J. 29 (1983) 552–560
2. **Balakotaiah, V.; Luss, D.:** Analysis of Multiplicity Patterns of a CSTR. Chem. Engng. Commun. 13 (1982) 111–124
3. **Abasaeed, A.E.; Elnashaie, S.S.E.H.:** On the chaotic behaviour of Externally forced Industrial Fluid Catalytic Cracking Units. Chaos, Solitons & Fractals. 9 (1998) 455–470
4. **Elnashaie, S.S.E.H.; Abasaeed, E.A.; Elshishini, S.S.:** Digital Simulation of Industrial Fluid Catalytic Cracking Units: V. Static and Dynamic Bifurcation Behaviour. Chem. Eng. Sci. 50 (1995) 1635–1644
5. **Uppal, A.; Ray, W.H.; Poore, A.B.:** On the Dynamic Behaviour of Continuous Stirred Tank Reactors. Chem. Eng. Sci. 29 (1974) 967–985
6. **Alhumaizi, K.; Aris, R.:** Chaos in a Simple Two-Phase Reactor. Chaos, Solitons & Fractals. 4 (1994) 1985–2014
7. **Gray, P.; Scott, S.K.:** Autocatalytic Reactions in the Isothermal, Continuous Stirred Tank Reactor. Isola and Other Forms of Multiplicity. Chem. Eng. Sci. 38 (1983) 29–43
8. **Gray, P.; Scott, S.K.:** Autocatalytic Reactions in the Isothermal, Continuous Stirred Tank Reactor. Oscillations and Instabilities in the System. Chem. Eng. Sci. 39 (1984) 1087–1097
9. **Peng, B.; Scott, S.K.; Showalter, K.:** Period-Doubling and Chaos in a Three-Variable Autocatalator. J. Phys. Chem. 94 (1990) 5243–5246
10. **Lynch, D.T.:** Chaotic Behavior of Reaction Systems: Parallel Cubic Autocatalator. Chem. Eng. Sci. 47 (1992) 347–355
11. **Lynch, D.T.:** Chaotic Behavior of Reaction Systems: Mixed Cubic and Quadratic Autocatalysis. Chem. Eng. Sci. 47 (1992) 4435–4444
12. **Leach, J.A.; Merkin, J.H.; Scott, S.K.:** An Analysis of a Two-Cell Coupled Nonlinear Chemical Oscillator. Dynamics and Stability of Systems 6 (1991) 341–365
13. **Doedel, E.J.; Kernevez, J.P.:** Auto: Software for continuation and bifurcation problems in ordinary differential equations. (1986) California Institute of Technology, CA, USA
14. **Wolf, A.; Swift, J.B.; Swinney, H.L.; Vastano, J.A.:** Determining Lyapunov Exponents from a Time Series. Physica 16D (1985) 285–317
15. **Pomeau, Y.; Manneville, P.:** Intermittent transition to turbulence in dissipative dynamical systems. Commun. Math. Phys. 74 (1980) 189–197
16. **Tambe, S.S.; Kulkarni, B.D.:** Intermittency route to chaos in a periodically forced model reaction system. Chem. Engng. Sci. 48 (1993) 2817–2821